MODIFICATION OF SLANT RANGE MODEL AND IMAGING PROCESSING IN GEO SAR

Cheng Hu[1], Feifeng Liu[2], Wenfu Yang[3], Tao Zeng[4]

[1,2,3,4] :Department of Electronic Engineering, Beijing Institute of Technology, P.R.China, 100081

1. INTRODUCTION

With the development of SAR application, the disadvantage of low earth orbit (LEO) SAR becomes more and more apparent. The increase of orbit altitude can shorten the revisit time and enlarge the coverage area in single look, and then satisfy the application requirement. The concept of geosynchronous earth orbit (GEO) SAR system is firstly presented by K.Tomiyasi in [1], and deeply discussed in [2-4]. A GEO SAR, with its fine temporal resolution, would overcome the limitations of current imaging systems, allowing dense interpretation of transient phenomena as GPS time-series analysis with a spatial density several orders of magnitude finer [3-4].

In the LEO SAR, the signal model analysis adopts the 'Stop-and-Go' assumption in general [5], and this assumption can satisfy the imaging requirement in present advanced SAR system [5], such as TerraSAR, Radarsat2 and so on. However because of long propagation distance and non-negligible earth rotation, the 'Stop-and-Go' assumption does not exist and will cause large propagation distance error, and then affect the image formation.

In this paper, considering the relative motion between satellite and earth during signal propagation time, the accurate analysis method for propagation slant range is firstly presented. Furthermore, the difference between accurate analysis method and 'Stop-and-Go' assumption is analytically obtained. Meanwhile based on the derived accurate slant range model, the corresponding range migration correction and azimuth reference function must consider the high order term, and therefore the modified SPECAN algorithm is proposed. The simulation results verify the correctness of 'Stop-and-Go' assumption error derivation and SPECAN algorithm modification.

2. THE ACCURATE SLANT RANGE MODEL

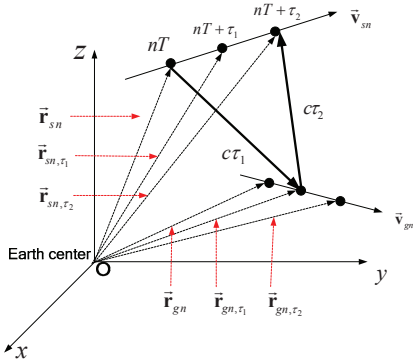

Fig. 1 The illustration of propagation range at nth PRT moment in GEO SAR

With the increase of the orbit altitude, especially in GEO SAR system, the single way propagation distance reaches to 40000km, namely that the two way propagation delay is close to the order of seconds, the GEO SAR velocity is near to 3000m/s, therefore the relative motion between satellite and target has to be considered, the 'Stop-and-Go' assumption no longer exists in GEO SAR. The illustration of propagation range in GEO SAR is shown in Fig. 1. In Fig. 1, the earth center is denoted as ordinate origin O, the Oxyz is the earth inertial coordinate system. At the nth transmitted pulse moment, the satellite moves with velocity $\vec{\mathbf{v}}_{sn}$; because of the earth rotation, the target stationary on the ground moves with velocity $\vec{\mathbf{v}}_{gn}$, the satellite position vector (SPV) and target position vector (TPV) are denoted as $\vec{\mathbf{r}}_{sn}$ and $\vec{\mathbf{r}}_{gn}$ respectively. After the propagation time τ_1, the transmitted signal impinges on the target and is reflected from the target, at this moment, the SPV and TPV are denoted as $\vec{\mathbf{r}}_{sn,\tau_1}$ and $\vec{\mathbf{r}}_{gn,\tau_1}$ respectively. The reflected signal reaches to the satellite via propagation time τ_2, at this moment, the SPV and TPV are denoted as $\vec{\mathbf{r}}_{sn,\tau_2}$ and $\vec{\mathbf{r}}_{gn,\tau_2}$ respectively. As we can see from Fig. 1, the total propagation range is equal to the sum of $c\cdot\tau_1$ and $c\cdot\tau_2$, and can be written as

$$\begin{cases} R_{sn} = R_{1n} + R_{2n} \\ R_{1n} = c\cdot\tau_1 = \left\| \vec{\mathbf{r}}_{sn} - \vec{\mathbf{r}}_{gn,\tau_1} \right\|_2, \qquad R_{2n} = c\cdot\tau_2 = \left\| \vec{\mathbf{r}}_{gn,\tau_1} - \vec{\mathbf{r}}_{sn,\tau_2} \right\|_2 \end{cases} \tag{1}$$

where c stands for the speed of light, the symbol '$\| \ \|_2$' is the norm operator, the symbol '$< >$' stands for the inner product operator. According to the relationship between position vector and velocity vector, we have

$$\begin{cases} \tau_1 = \left[\sqrt{\left\langle \vec{\mathbf{r}}_{sn} - \vec{\mathbf{r}}_{gn}, \vec{\mathbf{v}}_{gn} \right\rangle^2 + \left(c^2 - \vec{\mathbf{v}}_{gn}\cdot\vec{\mathbf{v}}_{gn}^T \right)\cdot\left\langle \vec{\mathbf{r}}_{sn} - \vec{\mathbf{r}}_{gn}, \vec{\mathbf{r}}_{sn} - \vec{\mathbf{r}}_{gn} \right\rangle} - \left\langle \vec{\mathbf{r}}_{sn} - \vec{\mathbf{r}}_{gn}, \vec{\mathbf{v}}_{gn} \right\rangle \right] \Big/ \left(c^2 - \vec{\mathbf{v}}_{gn}\cdot\vec{\mathbf{v}}_{gn}^T \right) \\ \tau_2 = \left[\sqrt{\left\langle \vec{\mathbf{r}}_{gn,\tau_1} - \vec{\mathbf{r}}_{sn,\tau_1}\cdot\vec{\mathbf{v}}_{sn} \right\rangle^2 + \left(c^2 - \vec{\mathbf{v}}_{sn}\cdot\vec{\mathbf{v}}_{sn}^T \right)\cdot\left\langle \vec{\mathbf{r}}_{gn,\tau_1} - \vec{\mathbf{r}}_{sn,\tau_1}, \vec{\mathbf{r}}_{gn,\tau_1} - \vec{\mathbf{r}}_{sn,\tau_1} \right\rangle} - \left\langle \vec{\mathbf{r}}_{gn,\tau_1} - \vec{\mathbf{r}}_{sn,\tau_1}\cdot\vec{\mathbf{v}}_{sn} \right\rangle \right] \Big/ \left(c^2 - \vec{\mathbf{v}}_{sn}\cdot\vec{\mathbf{v}}_{sn}^T \right) \end{cases} \tag{2}$$

From the eq.(2), the propagation delay can be accurately calculated, but the expression is very complex, therefore it is necessary to simplify the eq.(2) concisely. Using the Taylor series expansion to eq.(2), after complex algebra computation, the propagation range shown in eq.(1) can be approximated as

$$R_{sn} = 2\cdot\left\| \vec{\mathbf{r}}_{sn} - \vec{\mathbf{r}}_{gn} \right\|_2 + \frac{2\cdot\left\langle \left(\vec{\mathbf{v}}_{sn} - \vec{\mathbf{v}}_{gn} \right), \left(\vec{\mathbf{r}}_{sn} - \vec{\mathbf{r}}_{gn} \right) \right\rangle}{c - \left\langle \left(\vec{\mathbf{v}}_{sn} - \vec{\mathbf{v}}_{gn} \right), \left(\vec{\mathbf{r}}_{sn} - \vec{\mathbf{r}}_{gn} \right) \Big/ \left\| \vec{\mathbf{r}}_{sn} - \vec{\mathbf{r}}_{gn} \right\|_2 \right\rangle} \tag{3}$$

The propagation range in eq.(3) is very close to the accurate propagation range in eq.(1), it is not difficult to find the error caused by the 'Stop-and-Go' assumption can be approximately expressed by the inner product of velocity difference vector and position difference vector, namely that

$$\Delta R_{sn} = \frac{2\cdot\left\langle \left(\vec{\mathbf{v}}_{sn} - \vec{\mathbf{v}}_{gn} \right), \left(\vec{\mathbf{r}}_{sn} - \vec{\mathbf{r}}_{gn} \right) \right\rangle}{c - \left\langle \left(\vec{\mathbf{v}}_{sn} - \vec{\mathbf{v}}_{gn} \right), \left(\vec{\mathbf{r}}_{sn} - \vec{\mathbf{r}}_{gn} \right) \Big/ \left\| \vec{\mathbf{r}}_{sn} - \vec{\mathbf{r}}_{gn} \right\|_2 \right\rangle} \tag{4}$$

According to the eq.(4), the 'Stop-and-Go' assumption error in GEO SAR is shown in Fig. 2. As we can see from Fig. 2, the 'Stop-and-Go' assumption error reaches to 80m at the equator in GEO SAR, it means that we must consider the range displacement during the range migration correction and azimuth compression processing.

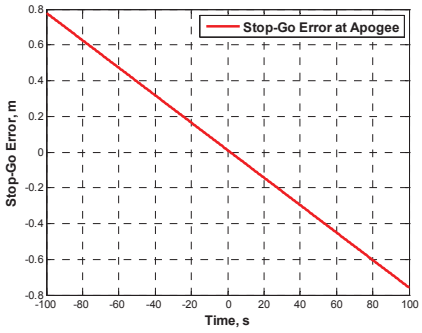

(a) The Stop-Go Error at apogee

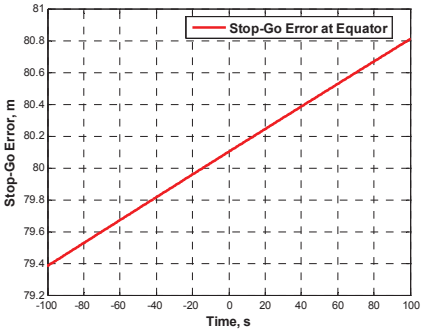

(b) The Stop-Go Error at Equator

Fig. 2 The Error between 'Stop-and-Go' assumption and accurate slant range model

3. THE MODIFIED IMAGING PROCESSING IN GEO SAR

According to the eq.(3), we know the accurate slant range in GEO SAR consists of two parts, one part is the slant range under the 'Stop-and-Go' assumption, the other part is ΔR_{sn}. Because the long synthetic aperture time in GEO SAR, considering the compromise of algorithm efficiency and accuracy, the SPECAN algorithm is chosen for the GEO SAR imaging processing. In conventional SPECAN algorithm, the range migration correction only uses the Doppler center to correct the range walk, the range curvature is ignored; furthermore, the azimuth dechirp processing only uses the second order reference function and neglects the high order phase. In GEO SAR system, the long synthetic aperture time results in the large range migration and long curve synthetic aperture, therefore the conventional SPECAN algorithm is collapsed, the modified SPECAN algorithm should be put forward. In the modified SPECAN algorithm, the rang migration correction considers the second order and third order range curvatures as well as 'Stop-and-Go' assumption error; the azimuth dechirp processing considers at least third order phase reference function. The mathematic expression can be written as

$$R_{migr}(nT) = \lambda \cdot (f_{dc} + \Delta f_{dc}) \cdot nT + \frac{\lambda}{2} \cdot (f_{dr} + \Delta f_{dr}) \cdot nT^2 + \frac{\lambda}{6} \cdot (f_{drr} + \Delta f_{drr}) \cdot nT^3 \tag{5}$$

$$H_{Az-ref}(nT) = \exp\left[-j2\pi (f_{dc} + \Delta f_{dc}) \cdot nT - j\pi (f_{dr} + \Delta f_{dr}) \cdot (nT)^2 - j\pi f_{drr} (nT)^3\right] \tag{6}$$

where $R_{migr}(nT)$ is the range migration correction expression, and $H_{Az-ref}(nT)$ is azimuth dechirp reference function. f_{dc}, f_{dr} and f_{drr} are the Doppler center frequency, Doppler chirp-rate and the rate of Doppler chirp-rate respectively. Δf_{dc}, Δf_{dr} and Δf_{drr} are the differences of corresponding parameters considering the 'Stop-and-Go' assumption. According to the system geometric parameters, we have

$$f_{dc} = 2 \cdot (\vec{\mathbf{v}}_{s0} - \vec{\mathbf{v}}_{g0}) \cdot \vec{\mathbf{u}}_{gs,0}^T / \lambda, \quad f_{dr} = \frac{2}{\lambda} \cdot \left[(\vec{\mathbf{a}}_{s0} - \vec{\mathbf{a}}_{g0}) \cdot \vec{\mathbf{u}}_{gs,0}^T + (\vec{\mathbf{v}}_{s0} - \vec{\mathbf{v}}_{g0}) \cdot (\mathbf{I} - \vec{\mathbf{u}}_{gs,0}^T \cdot \vec{\mathbf{u}}_{gs,0}) \cdot (\vec{\mathbf{v}}_{s0} - \vec{\mathbf{v}}_{g0})^T / \left\| \vec{\mathbf{r}}_{s0} - \vec{\mathbf{r}}_{g0} \right\|_2 \right] \tag{7}$$

$$\Delta f_{dc} = 2 \cdot \left[\left\langle (\vec{\mathbf{a}}_{s0} - \vec{\mathbf{a}}_{g0}), (\vec{\mathbf{r}}_{s0} - \vec{\mathbf{r}}_{g0}) \right\rangle + \left\langle (\vec{\mathbf{v}}_{s0} - \vec{\mathbf{v}}_{g0}), (\vec{\mathbf{v}}_{s0} - \vec{\mathbf{v}}_{g0}) \right\rangle \right] / (c \cdot \lambda) \tag{8}$$

$$\Delta f_{dr} = 2 \cdot \left[\left\langle (\vec{\mathbf{b}}_{s0} - \vec{\mathbf{b}}_{g0}), (\vec{\mathbf{r}}_{s0} - \vec{\mathbf{r}}_{g0}) \right\rangle + 2 \cdot \left\langle (\vec{\mathbf{a}}_{s0} - \vec{\mathbf{a}}_{g0}), (\vec{\mathbf{v}}_{s0} - \vec{\mathbf{v}}_{g0}) \right\rangle \right] / (c \cdot \lambda) \tag{9}$$

where $\vec{\mathbf{r}}_{s0}$ and $\vec{\mathbf{r}}_{g0}$ are the satellite and target position vectors at aperture center moment (ACM), $\vec{\mathbf{v}}_{s0}$ and $\vec{\mathbf{v}}_{g0}$ are the satellite and target velocity vectors at ACM, $\vec{\mathbf{a}}_{s0}$ and $\vec{\mathbf{a}}_{g0}$ are the satellite and target acceleration vector at ACM, $\vec{\mathbf{b}}_{s0}$ and $\vec{\mathbf{b}}_{g0}$ are the derivatives of $\vec{\mathbf{a}}_{s0}$ and $\vec{\mathbf{a}}_{g0}$ at ACM. c is the speed of light. $\vec{\mathbf{u}}_{gs,0}$ is line of sight (LOS) vector between satellite and target at ACM. $\mathbf{I}$ is the unity matrix, the superscript T means transpose. f_{drr} and Δf_{drr} are the derivatives of eq.(7) and eq.(9), here we don't give the detail expression because of the page limitation.

4. SIMULATION RESULTS

In order to verify the correctness of above derivation, the simulation parameters are as below: the satellite height is 36000km; the eccentricity is 0.07; the nadir point is on the equator; the downing looking angle is 4.65 degrees; the transmitted signal bandwidth is 18MHz; the sampling frequency is 20MHz; the synthetic aperture time is 400 seconds; the pulse repetition frequency (PRF) is 300Hz and the signal wavelength is 0.09 meter. The imaging results of classic SPECAN and modified SPECAN algorithm are shown in Fig.3 and Fig.4.

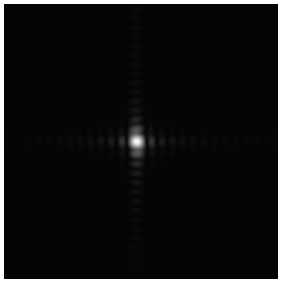

(a) The imaging results of point target

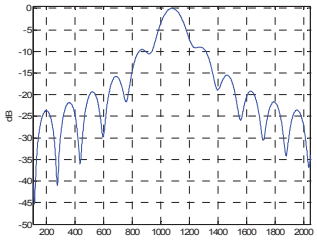

(b) The azimuth profile of point target imaging

Fig. 3 The classic SPECAN algorithm imaging

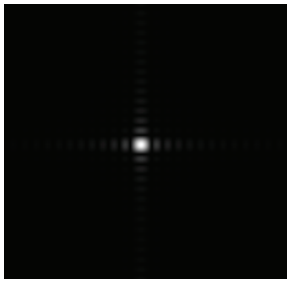

(a) The imaging results of point target

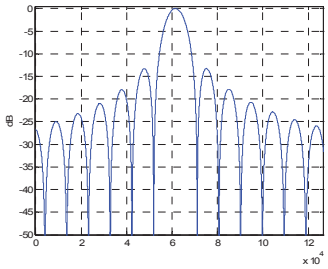

(b) The azimuth profile of point target imaging

Fig. 4 The modified SPECAN algorithm imaging

As we can see from Fig.3, when the classic SPECAN algorithm is used, the azimuth direction can not be well focused and the peak to side-lobe ratio (PSLR) increases to -10dB (shown in Fig.3-b). From Fig.4 when the modified SPECAN algorithm is used, the good imaging results are obtained and the azimuth direction is well focused (shown in Fig.4-b). Therefore the imaging results verify the correctness and essential of SPECAN algorithm modification.

5. REFERENCES

[1] Tomiyasu, Kiyo; Synthetic aperture radar in geosynchronous orbit. Dig.Int. IEEE Antennas and Propagation Symp., U.Maryland, pp.42-45, May 1978.

[2] Tomiyasu, Kiyo; Pacelli, Jean L.; Synthetic Aperture Radar Imaging from an Inclined Geosynchronous Orbit. Geoscience and Remote Sensing, IEEE Transactions on, Volume GE-21, Issue 3, July 1983 Page(s):324 – 329.

[3] Madsen, S.N.; Chen, C.; Edelstein, W.; Radar options for global earthquake monitoring. Geoscience and Remote Sensing Symposium, 2002. IGARSS '02. 2002 IEEE International, Volume 3, 24-28 June 2002 Page(s):1483 - 1485 vol.3.

[4] Moussessian, A.; Chen, C.; Edelstein, W.; Madsen, S.; Rosen, P.; System concepts and technologies for high orbit SAR. Microwave Symposium Digest, 2005 IEEE MTT-S International 12-17 June 2005, pp 1623-1626.

[5] J.C.Curlander and R.N.McDonough, Synthetic aperture radar: Systems and signal processing, New York, USA: John Wiley&Sons, 1991.